Spreading of a granular mass on a horizontal plane

Cite as: Physics of Fluids **16**, 2371 (2004); https://doi.org/10.1063/1.1736611
Submitted: 04 December 2003 • Accepted: 08 March 2004 • Published Online: 27 May 2004

E. Lajeunesse, A. Mangeney-Castelnau and J. P. Vilotte

Spreading of a granular mass on a horizontal plane

E. Lajeunesse
Laboratoire de Dynamique des Systèmes Géologiques, Groupe de Recherches sur l'Erosion et les Eaux Continentales, Institut de Physique du Globe de Paris, 4 place Jussieu, 75252 Paris Cedex 05, France

A. Mangeney-Castelnau and J. P. Vilotte
Départment de Sismologie, Institut de Physique du Globe de Paris, 4 place Jussieu, 75252 Paris Cedex 05, France

(Received 4 December 2003; accepted 8 March 2004; published online 27 May 2004)

The transient surface flow occurring when a cylindrical pile of dry granular material is suddenly allowed to spread on a horizontal plane is investigated experimentally as a function of the released mass M, the initial aspect ratio a of the granular cylinder pile, the properties of the underlying substrate (smooth or rough, rigid or erodible) and the bead size. Two different flow regimes leading to three different deposit morphologies are observed as a function of the initial aspect ratio a, whatever the substrate properties and the bead size. For $a \lesssim 3$, the granular mass spreads through an avalanche on its flanks producing either truncated cone or conical deposits. For $a \gtrsim 3$, the upper part of the column descends conserving its shape while the foot of the pile propagates radially outward. The obtained deposit looks like a ''Mexican hat'' and the slope angle at the foot of the deposit is observed to saturate at a value of the order of 5°. For a given ground and bead size, the flow dynamics and the deposit morphology are found to be independent of M and to vary only with the initial aspect ratio a. Further investigation indicates that the deposit morphology depends only slightly on the substrate properties and the bead size, except when a becomes large. In particular the same dynamical regimes and deposit morphologies are recovered for the same range of a, independent of the substrate properties or the bead size. Moreover the rescaled deposit radius, the rescaled spreading velocity, and the fraction of energy dissipated during the flow do not depend on M, the substrate properties, or the bead size, but vary only with a. We believe this to be the signature of the fact that the flow develops near the free surface of the granular pile so that the dynamics is essentially controlled by grain/grain interactions.
[DOI: 10.1063/1.1736611]

I. INTRODUCTION

Geophysical granular mass flows such as rock avalanches or debris flows consist in the flow of a mass of solid grains surrounded by a less dense intergranular fluid such as water or gas.[1,2] The volumetric concentration of grains is usually high enough for interparticle forces to dominate momentum transport.[2] In that case the effect of the intergranular fluid is negligible so that dry granular flows therefore constitute a useful paradigm to study these kinds of geophysical events.

Most of the experimental studies devoted to granular flows have focused on the flow of a granular material along inclines of slope larger than the material repose angle.[3–5] In this configuration, the flow is driven by the component of gravity along the slope direction and the flow thickness is usually small enough to permit the use of hydrodynamic models based on the depth averaged Saint–Venant approach.[6,7] Such hydrodynamic models have been successfully applied to the description of some geophysical granular flow events.[8–10]

Another configuration of interest in nature is that where a granular mass is suddenly released on a quasi-horizontal surface, as in a cliff collapse. In that situation the granular mass is expected to crumble and spread under its own weight. To our knowledge, only a few studies have addressed comparable situations. Boutreux and de Gennes[11] discussed the evolution of a step of dry granular matter spreading through an avalanche in the frame of the BCRE equations[12] and concluded that the final slope angle should be smaller than the repose angle. More recently, Daerr and Douady[13] investigated experimentally the effect of the packing density on the transient granular surface flow occurring when a cylindrical pile of dry granular media supported by a disc is suddenly released and crumbles to form a cone.

Despite these studies, the flow of a dry granular mass suddenly released on a horizontal surface remains a challenging problem which raises several questions. What fraction of the granular mass is mobilized by the flow? What controls the flow dynamics? What is the shape of the resulting deposit? In this paper, we report the results of an experimental study addressing some of these questions. The experimental procedure is very simple: a mass of dry granular material enclosed inside a tube is suddenly allowed to spread on a horizontal plane upon removal of the tube. The spreading dynamics and the morphology of the resulting deposit are investigated experimentally as a function of the released mass, the initial aspect ratio of the granular cylinder pile, the properties of the underlying substrate (smooth or rough, rigid

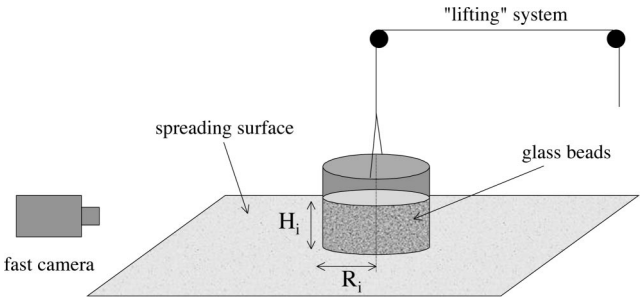

FIG. 1. Scheme of the experimental setup.

or erodible), and the bead size. Our objective is to identify the main parameters controlling the flow dynamics and the shape of the resulting deposit in this simple and well-controlled geometry.

The paper is organized as follows. The experimental setup and procedure are described in Sec. II. The experimental results are reported and discussed in Sec. III. The paper ends with a summary of the results and conclusions.

II. EXPERIMENTAL SETUP AND PROCEDURE

The experimental setup displayed in Fig. 1 consists of a cylinder of inner radius R_i resting on a horizontal 60 cm $\times$60 cm plane. The tube is partially filled with a mass M of glass beads of diameter $d=350\pm50\,\mu$m so as to form a column of radius R_i and height H_i. The repose and avalanche angles θ_r and θ_a of our granular material were roughly estimated from the variations of the slope along a granular pile built by slowly pouring beads from a small height. We found $\theta_r\approx21°$ and $\theta_a\approx29°$.

To ensure reproducible initial conditions, the tube was always filled following the same procedure: the glass beads are poured via a funnel onto a sieve placed above the tube, resulting in a homogeneous downfall of grains. The mean density of packing of the granular column was roughly estimated by $\phi=M/(\rho_0\pi R_i^2 H_i)$ where $\rho_0=2500\,\mathrm{kg/m^3}$ is the density of the glass beads. ϕ was found to vary between 0.62 and 0.65 indicating dense initial heaps.[13]

The experimental procedure simply consists in quickly removing the tube by means of a lifting system made of rope and pulleys. After it is released, the granular mass spreads on the horizontal plane until it comes to rest and forms a deposit. It is important to note that the experimental protocol is valid only if the time T_r necessary to release the granular mass remains small compared to the time T_m necessary to set the granular mass in motion. T_m can be roughly estimated as $T_m=\sqrt{2H_i/g}$ where H_i is the initial height of the granular mass. The release time is of the order of $T_r=H_i/V_{\mathrm{lift}}$, where V_{lift} is the lifting velocity of the tube, on the order of $V_{\mathrm{lift}}\approx1.6\,\mathrm{m\,s^{-1}}$. As a consequence, the experimental protocole is valid provided that the initial height of the granular column H_i is small compared to $2V_{\mathrm{lift}}^2/\mathrm{g}\approx50\,\mathrm{cm}$. In practice, H_i was varied from 0.7 to 25 cm.

The time evolution of the granular mass was measured by means of a 1024$\times$1024 pixel digital camera acquiring 500 images per second. A first series of experiments conducted with the camera placed vertically above the experimental setup allowed us to verify that the granular mass spreads axisymmetrically. In all other experiments the camera was carefully aligned along the horizontal direction so as to acquire side views of the granular mass. The spatial resolution achieved in these conditions is 0.4 mm per pixel. The camera was connected to a computer and the digitized images were processed in order to extract the profiles $h(r,t)$ of the granular mass throughout time t, h being the local thickness and r the radial distance to the axis of symmetry of the granular mass. As the granular mass spreads axisymmetrically, its profile provides enough information to fully characterize its three-dimensional shape.

TABLE I. Characteristics of the different series of experiments.

Series	d	Substrate
1	350 ± 50 μm	Sandpaper of roughness $\lambda\approx540$ μm
2	350 ± 50 μm	Erodible bed (same granular material) of thickness 4 or 12 mm
3	350 ± 50 μm	Smooth wooden surface
4	1150 ± 150 μm	Sandpaper of roughness $\lambda\approx540$ μm

III. EXPERIMENTAL RESULTS

Several series of experiments were conducted in order to study the effect of different control parameters namely: the released mass M, the initial aspect ratio of the granular column defined as $a=H_i/R_i$, the properties of the substrate on which the beads are spreading (rigid or erodible, rough or smooth) and the bead size. The characteristics of these different series are summarized in Table I.

In a first series of experiments, glass beads of diameter $d=350\pm50\,\mu$m were released on a horizontal plane covered with sandpaper of roughness of the order of $\lambda\approx540$ μm. A large number of experiments were conducted where the mass M was varied from 25 g to 3.5 kg and the aspect ratio a was varied from 0.2 up to 20. This was achieved by using four different tubes of inner radius 13, 28, 40, and 70.5 mm, respectively.

A second set of experiments was performed in order to study the effect of an erodible bed on the spreading flow dynamics. This time, the same beads were released on a horizontal static layer of the same material. The effect of the thickness of the erodible bed was also investigated by working with beds of two different thicknesses, namely 4 and 12 mm. No difference of flow dynamics and deposit morphology was observed between these two sets of experiments. In the following, we will therefore not discuss the effect of the thickness of the erodible ground and concentrate on the differences observed between rigid and erodible ground.

The influence of the ground roughness was briefly investigated by performing a third series of experiments which consisted in releasing the same beads on a wooden surface much smoother than the sandpaper substrate. Note that neither the wooden surface roughness nor that of the sandpaper were precisely measured and characterized. As a result our analysis of the influence of the ground roughness is essentialy qualitative.

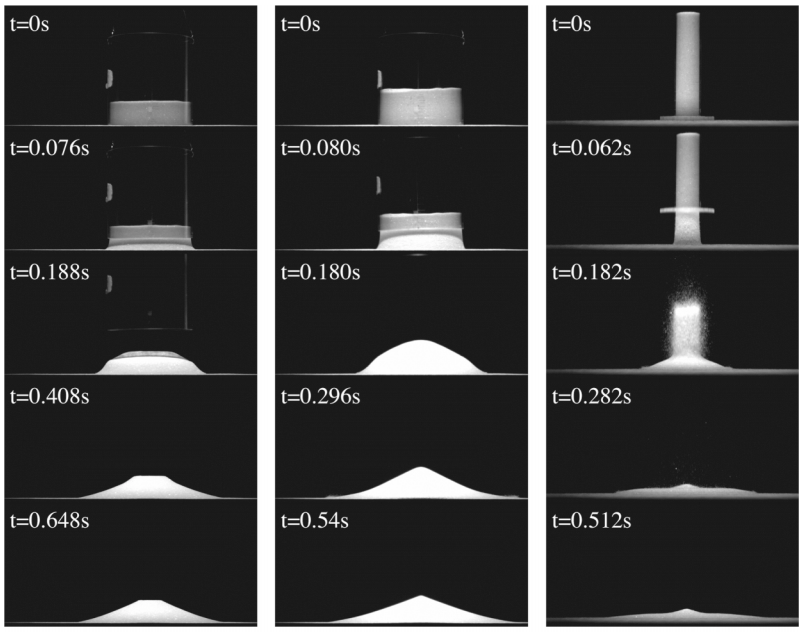

FIG. 2. Three sequences of images corresponding to $d=350\ \mu$m beads spreading on a sandpaper substrate of roughness $\lambda\approx 540\ \mu$m. (a) Regime 1, $a=0.56$, $M=950$ g, $R_i=70.5$ mm. (b) Regime 1, $a=0.8$, $M=1450$ g, $R_i=70.5$ mm. (c) Regime 2, $a=5.4$, $M=600$ g, $R_i=28$ mm.

Finally, the effect of bead size was investigated by performing a few experiments where beads of diameter $d=1150\pm 150\ \mu$m were released on the sandpaper substrate of roughness $\lambda\approx 540\ \mu$m.

In Secs. III A–III C we concentrate on the result of the two first series of experiments involving beads of diameter $d=350\pm 50\ \mu$m spreading either on the sandpaper substrate or on an erodible bed. We discuss how M, a, and the rigid or erodible nature of the rough ground affect the flow dynamics and the deposit morphology. The series of experiments 3 and 4 focusing on the influence of the substrate roughness and of the bead size are briefly discussed in Secs. III D and III E.

A. Qualitative description of the experiments

Depending on the value of the initial aspect ratio a of the released granular mass, we observed two distinctive dynamical regimes leading to three distinctive deposit morphologies. These dynamical regimes and the associated deposit morphologies are illustrated by the three sequences of images displayed in Fig. 2 and by the corresponding series of successive profiles displayed in Fig. 3. Although these data were obtained in the particular case of the first series of experiments where glass beads of diameter $d=350\pm 50\ \mu$m spread on the sandpaper substrate, the same qualitative behavior is observed in all our experimental series on rigid or erodible ground, whatever the beads' diameter or the ground roughness.

The first regime observed for $a\lesssim 3$ is illustrated in Figs. 2(a), 2(b), 3(a), and 3(b). Upon removal of the tube, the margins of the granular mass crumble through an avalanche. A flow front develops at the foot of the pile and propagates radially outward [see Figs. 3(a) and 3(b)]. In the meantime, a rear ''starting'' front separating the frontal flowing region from the summital motionless region propagates inward as is usually observed in dam break type situations.[14] Note the presence of an edge along the interface particularly visible on the $t=0.188$ s image of Fig. 2(a) and the $t=0.180$ s image of Fig. 2(b). This edge, which separates a steep frontal region from a summital region where the slope is smaller, remains located at the initial position $r=R_i$ of the edges of the granular column and progressively vanishes. Once the flow front has ceased to move, a ''stopping'' front separating an external region at rest from an internal still moving region forms and propagates inward. In this first regime, two different deposit morphologies are encountered depending on a. For $a<0.74$ the flow completely stops before the central undisturbed region has been completely consumed by the avalanche [see Figs. 2(a) and 3(a)]. As a result, the final deposit has roughly the shape of a ''truncated cone'' of height $H_f=H_i$ and of angle close to the repose angle of the beads $\theta_r=21°$. For $0.74<a\lesssim 3$, the avalanche completely consumes the central undisturbed region as shown in Fig. 3(b). As a result the final deposit has a conical shape of height H_f smaller than H_i [see Figs. 2(b) and 3(b)].

The flow dynamics of the second regime observed for $a\gtrsim 3$ is very different from that of the first one as visible in Fig. 2(c). Upon removal of the tube, the whole upper surface of the granular column starts to move instantaneously. Once again, a flow front develops at the foot of the pile and propagates radially outward. In the meantime the upper part of the column conserves its shape while descending [see Fig. 3(c)]. The whole pile comes at rest in a time interval smaller than the acquisition frame rate (0.02 s). The final deposit profile looking like a ''Mexican hat'' is made of a large almost flat outer region and a steep central cone.

Note that in the first regime the curvature of the deposit profile is positive all along the profile. On the contrary, the second regime deposits are characterized by the presence of an inflexion point separating an outer region where the curvature is negative from a central cone where the curvature is positive. The appearance of this inflexion point has therefore been chosen as a criterion to distinguish regime 2 from re-

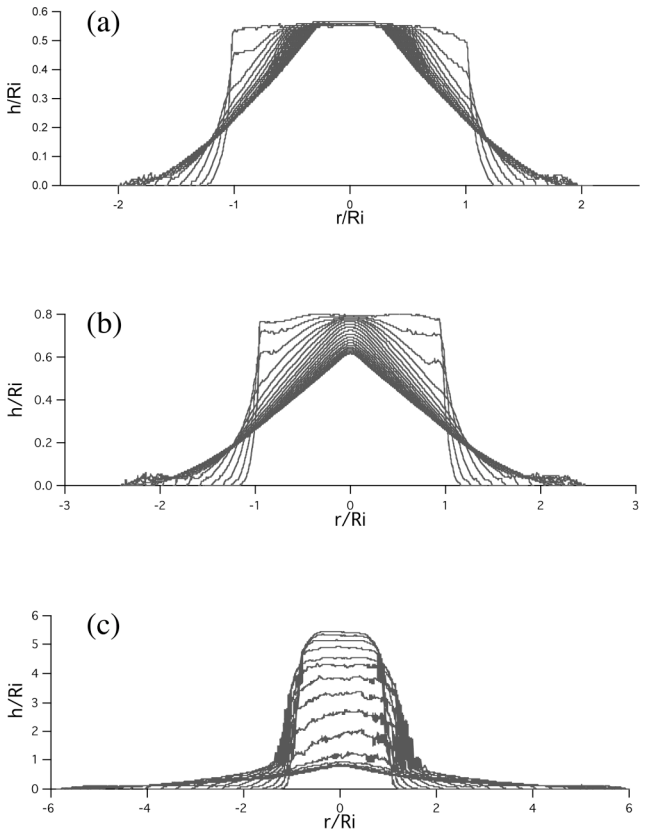

FIG. 3. Series of successive profiles $h(r,t)$ normalized to the tube radius R_i and corresponding to the images displayed in Fig. 2. The time lapse between two consecutive profiles is 0.02 s. (a) Regime 1, $a=0.56$, $M=950$ g, $R_i=70.5$ mm. (b) Regime 1, $a=0.8$, $M=1450$ g, $R_i=70.5$ mm. (c) Regime 2, $a=5.4$, $M=600$ g, $R_i=28$ mm.

gime 1. In practice, however, the presence of this inflexion point is sometimes difficult to detect so that the transition between regimes 1 and 2 is only approximately determined to occur when a is close to 3.

Acquiring side views of the pile is not completely satisfying as this does not allow us to observe the characteristics of the flow inside the granular mass. This difficulty was partially circumvented by applying the following procedure to a few experimental runs. The tube was alternatively filled with layers of white and red beads achieving an initial condition such as the one shown in Fig. 4(a). Once the granular mass has spread, the deposit is carefully split in two parts by means of a thin glass plate [Fig. 4(b)]. Removing one half of the deposit allows us to observe its internal structure through the glass plate as shown in Fig. 4(c). This particular example was obtained in the first regime with $a=1$, $M=1600$ g, $R_i=70.5$ mm, and $d=350\pm50$ μm. However the same behavior is observed in the second regime. The most obvious result is that the region of the granular mass located inside a cone visualized by the boundary plotted in dotted lines is not affected by the flow. In other words, the granular column reacts to the removal of the tube by developing a surface flow along its edges while the bulk remains static. Another interesting feature is that the different layers do not cross: the highest layers progressively cover over the lowest ones.

B. Effect of the mass, the initial aspect ratio, and the rigid/erodible nature of the spreading surface on the deposit morphology

Figure 5(a) displays three truncated cone deposit profiles $h(r)$ obtained for the same initial aspect ratio $a=0.41$ (regime 1) and with the same bead diameter $d=350\pm50$ μm. Whereas profiles 1 (plain lines, $M=135$ g, $R_i=40$ mm) and 2 (dotted lines, $M=50$ g, $R_i=28$ mm) are obtained on the rigid sandpaper substrate, profile 3 (plain lines with circles, $M=50$ g, $R_i=28$ mm) is obtained on an erodible bed. In order to compare these profiles corresponding to different values of M, h and r have been normalized with respect to R_i. Surprisingly the three normalized profiles perfectly match.

The same observation applies to both regime 1 conical and regime 2 ''Mexican-hat'' deposits as illustrated in Figs. 5(b) and 5(c). Normalized deposit profiles obtained for different masses and on erodible or rigid grounds match provided they correspond to the same initial aspect ratio a. Some more experimental runs varying M, a and working on erodible or rigid ground confirm these observations. First of all, under identical ground conditions, the shape of the deposit does not depend on the mass released but only on the initial aspect ratio a of the granular column. Second, the morphology of the deposits obtained on an erodible bed is similar to that obtained on a rigid sandpaper substrate of roughness $\lambda=540$ μm. This second result might be a consequence of the fact that the roughness of the rigid ground is slightly larger than the bead size. When spreading on the rough ground, part of the beads remains blocked in the large holes thus creating an apparent erodible bed of roughness equal to the size of the beads $d=350$ μm. Note also that the flow develops near the free surface of the granular pile (see Fig. 4) so that this later is essentially controlled by grain/grain interactions. This last argument suggests that the role played by the underlying rigid ground is negligible. This fact will be discussed in Sec. III D.

The deposit morphology being independent of M and of the rigid/erodible nature of the rough ground, we will now focus on the changes of deposit morphology when a is varied by measuring for each experimental run the height H_f, the radius R_f, and the local slope angle both at the foot and the summit of the deposit, respectively denoted α_f and α_s (see the inset of Fig. 6 for the definition of these quantities).

Figure 6(a) displays the rescaled deposit height H_f/R_i as a function of a. The different symbols correspond to the different experimental configurations investigated so far, that is for beads of diameter $d=350\pm50$ μm spreading either on a rigid sandpaper surface of roughness $\lambda=540$ μm or on an erodible bed. The two vertical dotted lines indicate the transitions between the different deposit morphologies. All the experimental data collapse on the same curve confirming that H_f/R_i depends only on a at leading order. For $a<0.74$, H_f/R_i increases linearly with a, which is of course a trivial consequence of the fact that $H_f=H_i$ in the case of a truncated-cone-like deposit. For $a>0.74$, H_f/R_i seems to roughly saturate at a value of the order of 0.74. To summarize:

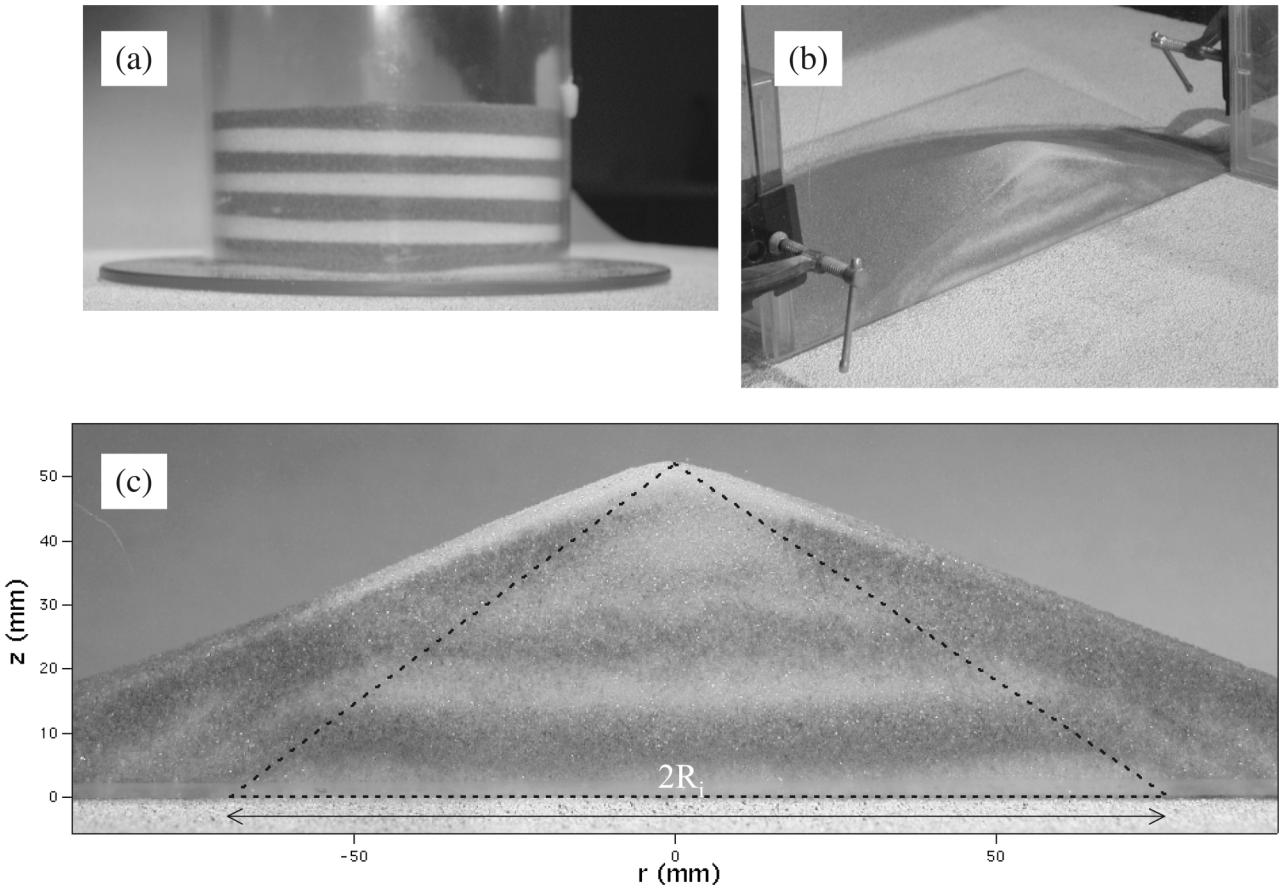

FIG. 4. Experimental procedure allowing us to explore the internal structure of the deposit. These images correspond to $a=1$, $M=1600$ g, $R_i=70.5$ mm, $d=350\pm50$ μm and the sandpaper substrate. (a) Initial state: the tube is alternatively filled with layers of white and red glass beads. (b) Deposit split in two parts by mean of a thin glass plate. (c) Internal structure of the deposit seen through the glass plate. The region of the granular mass located inside a cone visualized by the boundary plotted in dotted lines is not affected by the flow, indicating that the latter remains concentrated near the pile surface. The boundary separating the no-flow region from the one where surface flow has occurred has roughly the shape of a cone with a base that of the initial granular column and a slope between 35° and 37°.

$$a<0.74, \quad H_f=H_i, \tag{1}$$

$$a>0.74, \quad H_f\approx 0.74R_i. \tag{2}$$

These two equations suggest that upon removal of the tube the granular column yields along a failure surface of angle $\theta_y\approx\tan^{-1}(0.74)\approx 36.5°$. Such an interpretation is actually supported by the observation of the internal structure of the deposit displayed in Fig. 4: the boundary separating the no-flow region from the one where surface flow has occurred has roughly the shape of a cone with a base that of the initial granular column and a slope between 35° and 37°. In the frame of this interpretation, the final shape of the deposit has to depend of the initial aspect ratio of the granular column. In fact for $a>0.74$, the surface failure is inscribed inside the initial granular column: all the matter initially located above the surface failure is set into motion and the final height of the deposit is therefore on the order of that of the summit of the yielding cone, that is $H_f\approx 0.74R_i$. On the other hand, if $a<0.74$, only the sides of the initial granular column collapse, leaving a central undisturbed region and producing a truncated cone deposit with $H_f=H_i$. The angle $\theta_y\approx 36.5°$ is much larger than both the repose and the avalanche angles of the granular material but is compatible with an interpretation in terms of active Coulomb yielding. In that situation, the granular pile is expected to fail along an angle of the order of $45°-\delta/2$ where δ is the internal friction angle of the granular material. The latter can be roughly estimated to be of the order of the repose angle leading to $\theta_y\approx 34.5°$, not far from the 36.5° observed experimentally. Note that Daerr and Douady[13] also proposed an interpretation in terms of active Coulomb yielding to account for their experimental observation of the transient granular surface flow occurring when a highly compacted cylindrical pile of granular media supported by a disc is suddenly released and crumbles to form a cone. Interestingly, the packing density of our initial granular column is found to vary between 0.62 and 0.65, i.e., precisely in the range for which Daerr and Douady reported an active Coulomb yielding of the material.

Let us now discuss the variation of the relative radius of the deposit R_f/R_i with a. R_f/R_i is plotted against a in Fig. 6(b) for the different experimental configurations investigated so far, that is for beads of diameter 350 ± 50 μm spreading either on a sandpaper substrate of roughness $\lambda=540$ μm or on an erodible bed. As expected, all the experimental data collapse on the same curve confirming that R_f/R_i depends only on a at leading order. R_f/R_i increases

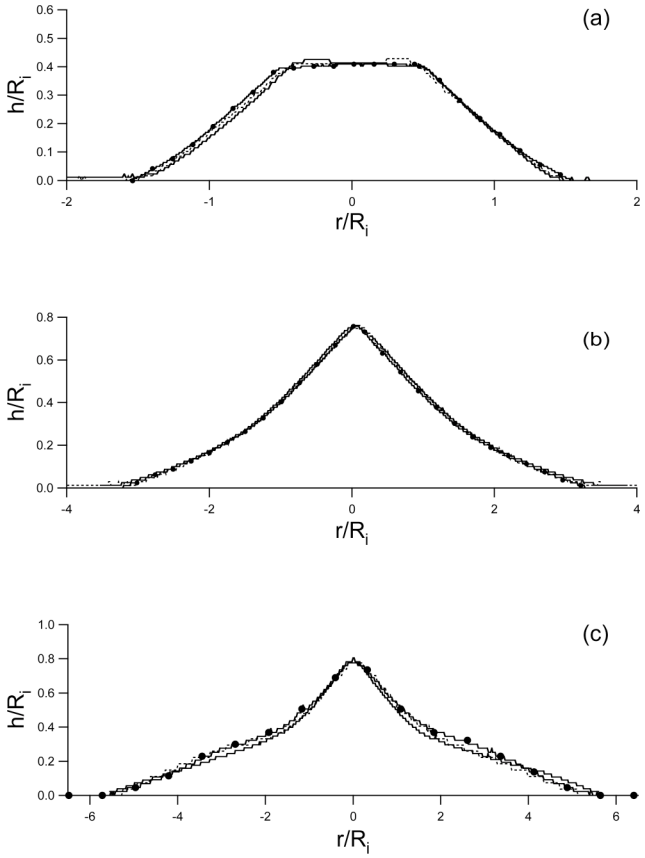

FIG. 5. Deposit profiles normalized to the tube radius obtained with bead of diameter $d=350\ \mu$m. (a) $a=0.41$. Plain line: $M=135$ g, $R_i=40$ mm, and rigid sandpaper substrate. Dotted line: $M=50$ g, $R_i=28$ mm, and rigid sandpaper substrate. Plain line with circles: $M=50$ g, $R_i=28$ mm, and erodible bed of thickness 4 mm. (b) $a=1.95$. Plain line: $M=600$ g, $R_i=40$ mm, and rigid sandpaper substrate. Dotted line: $M=200$ g, $R_i=28$ mm, and rigid sandpaper substrate. Plain line with circles: $M=600$ g, $R_i=40$ mm, and erodible bed of thickness 4 mm. (c) $a=6.2$. Plain line: $M=675$ g, $R_i=28$ mm, and rigid sandpaper substrate. Dotted line: $M=75$ g, $R_i=13$ mm, and rigid sandpaper substrate. Plain line with circles: $M=80$ g, $R_i=13$ mm, and erodible bed of thickness 4 mm.

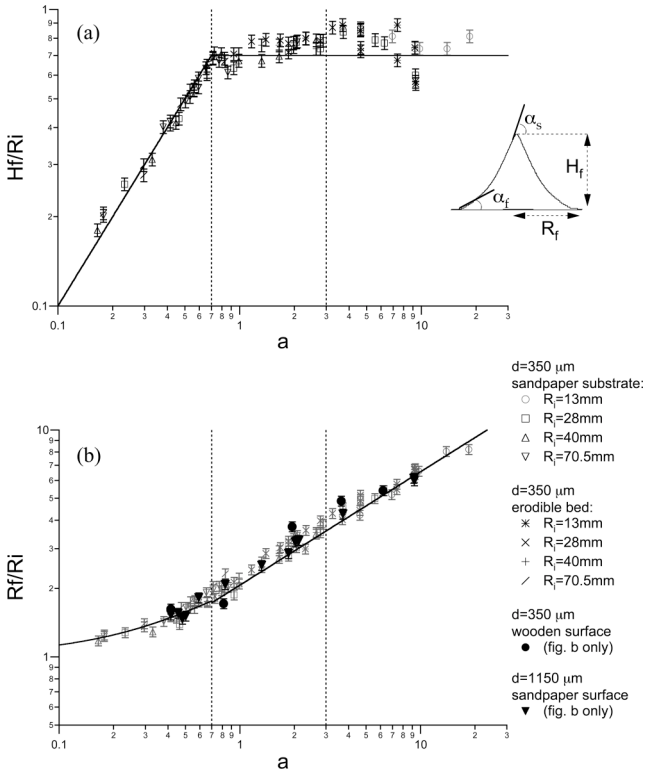

FIG. 6. (a) Rescaled height H_f/R_i and (b) rescaled radius R_f/R_i of the deposits as a function of a. The different symbols listed correspond to the different experimental configurations investigated with beads of diameter $350\pm50\ \mu$m spreading either on a sandpaper substrate of roughness $\lambda=540\ \mu$m or on an erodible bed. Data obtained with beads of diameter $350\pm150\ \mu$m spreading on a smooth wooden surface (solid circles) and beads of diameter $1150\pm150\ \mu$m spreading on the rigid sandpaper surface (solid triangles) have been added to (b). The vertical dotted lines indicate the transitions between the different deposit morphologies. The plain line in (a) corresponds to a fit of the experimental data whereas the plain line in (b) corresponds to the semi-empirical equations (4) and (5).

with a and is not affected by the changes of spreading flow regime.

Using mass conservation, geometrical arguments, and Eqs. (1) and (2), it is possible to account for the variation of R_f/R_i with a. In fact, for $a<0.74$, the deposit has the shape of a truncated cone of height $H_f=H_i$ and of angle close to the repose angle of the beads $\theta_r=21°$ so that its volume V_f is

$$V_f=\pi H_i^3\left(\frac{1}{3\mu_r^2}-\frac{1}{\mu_r}\frac{R_f}{H_i}+\left(\frac{R_f}{H_i}\right)^2\right), \tag{3}$$

where $\mu_r=\tan\theta_r$. As a result of mass conservation, the volume of the deposit V_f must be equal to that of the initially released granular column $V_i=\pi R_i^2 H_i$. Equating these two volumes leads to the following expression for R_f:

$$a<0.74,\quad \frac{R_f}{R_i}=\frac{1}{2\mu_r}\left(a+\sqrt{4\mu_r^2-\frac{a^2}{3}}\right). \tag{4}$$

For $a>0.74$, the deposit can be roughly approximated by a cone of volume $V_f=\pi H_f R_f^2/3$. Equating V_f and V_i and replacing H_f by (2) leads to

$$a>0.74,\quad \frac{R_f}{R_i}=\sqrt{\frac{3a}{0.74}}. \tag{5}$$

The semi-empirical equations (4) and (5) plotted in Fig. 6(b) (plain line) are found to be in a reasonably good agreement with the experimental data.

The shape of the deposit was also characterized by measuring α_s and α_f, the slope angles at the summit and at the foot of the deposit, respectively. This was achieved by a linear fit of the deposit profile near the summit and the foot, respectively. In the case of truncated cones, the summit of the deposit is flat. In that case we chose therefore to define α_s as the slope angle right below the edge of the summital plateau. The results are plotted against a in Figs. 7(a) and 7(b). In both cases, the data obtained in various experimental conditions collapse on the same curve indicating that α_s and α_f do not depend on the mass or on the rigid or erodible nature of the ground. α_s is observed to decrease logarithmically with a starting from a value of the order of $\alpha_s=27°$ for $a=0.2$ and decreasing to $\alpha_s\approx15°$ for $a=15$. The transition between truncated-cone deposits and conical deposits ap-

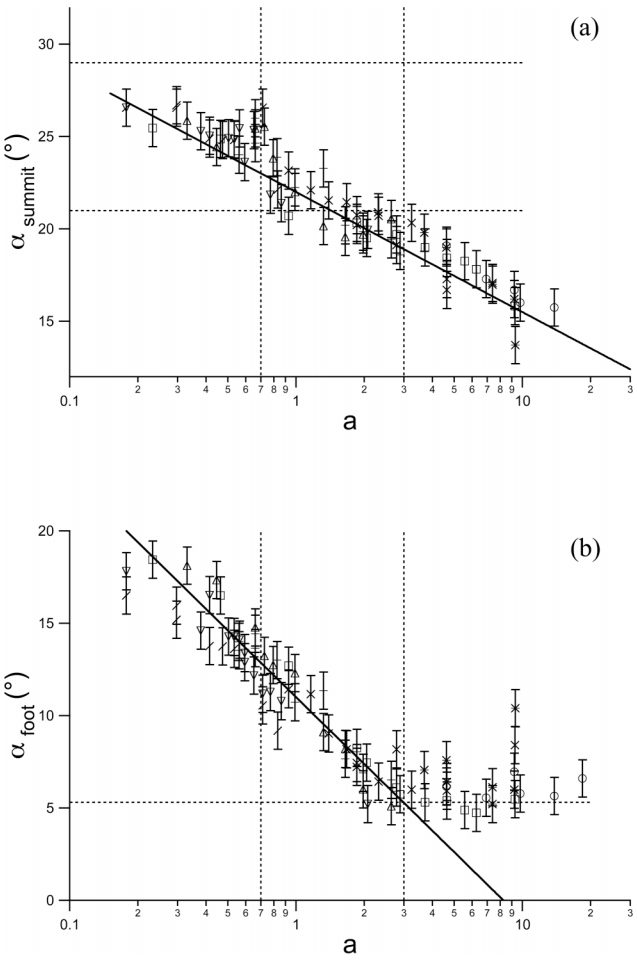

FIG. 7. Local slope angle (a) α_s at the summit of the deposit and (b) α_f at the foot of the deposit vs a. The different symbols refer to the same experimental configurations as in Fig. 6(a). In the case of truncated cones, α_s is defined as the slope angle right below the edge of the summital plateau.

proximately corresponds to the aspect ratio for which α_s becomes smaller than the repose angle $\theta_r = 21°$. The foot angle α_f is observed to remain smaller than θ_r in all our experiments. In the first regime, α_f decreases logarithmically with a. Interestingly the transition toward the second regime at $a \approx 3$ coincides with the saturation of α_f at a value on the order of 5°. Note that the observation of angles smaller than the repose angle is in agreement with the predictions of Boutreux and de Gennes.[11]

C. Effect of the mass, the initial aspect ratio, and the rigid/erodible nature of the spreading surface on the flow dynamics

The flow dynamics were investigated by tracking through time the position $r_f(t)$ of the foot of the granular pile as defined in the inset of Fig. 8. Except for a rapid transient acceleration at the beginning and a rapid transient deceleration at the end of the flow, the rim is observed to move at a nearly constant spreading velocity V during a relatively long time interval so that $r_f(t)$ exhibits an S shape as illustrated in Fig. 8. For each experimental run, we systematically measured the spreading velocity V when it is maximum by a linear fit of $r_f(t)$ in the vicinity of the inflexion point. The resulting velocities normalized by $\sqrt{gR_i}$ are plotted against a in Fig. 9(a). Once again, all the data collapse on the same curve: the rescaled spreading velocity $V/\sqrt{gR_i}$ depends neither on the mass released nor on the erodible or rigid nature of the ground but only on the initial aspect ratio a of the released mass. As already mentioned, this absence of difference between the rigid sandpaper surface of roughness $\lambda = 540$ μm and an erodible bed might be due to the fact that the roughness of the rigid ground is slightly larger than the bead size. When spreading on the rough ground, part of the

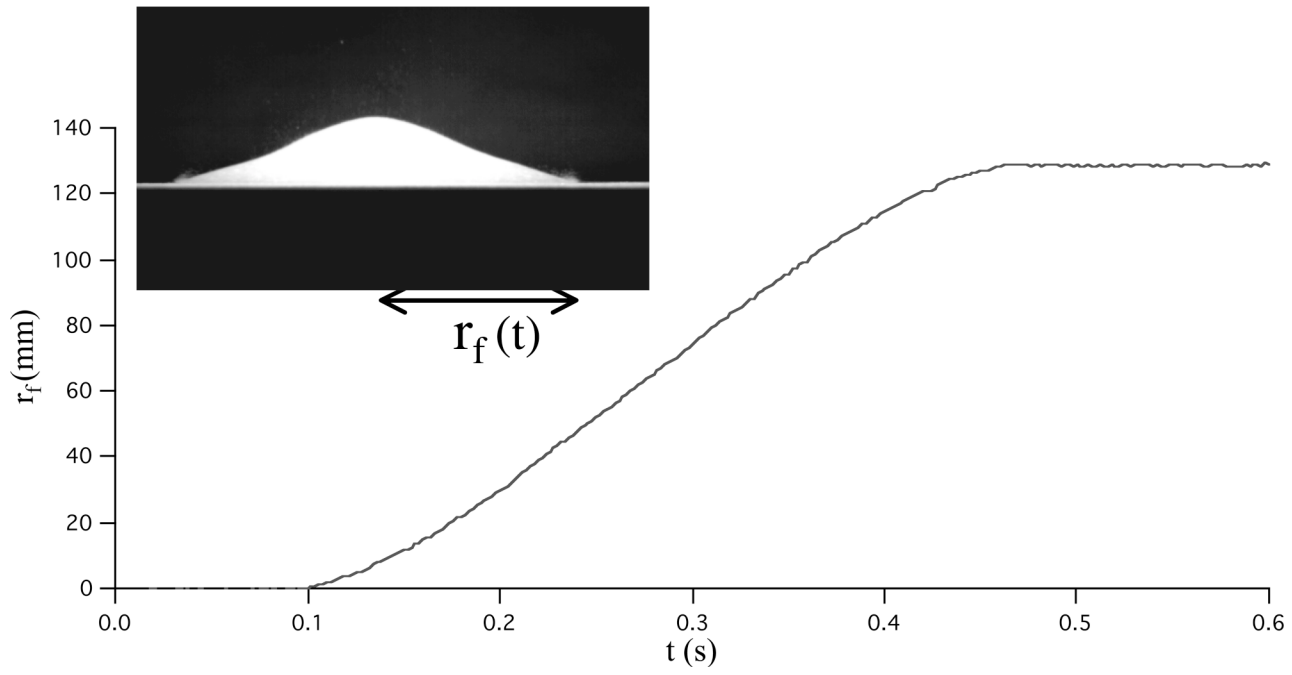

FIG. 8. Position $r_f(t)$ of the foot of the spreading granular pile through time ($d = 350$ μm, $a = 5.4$, $M = 600$ g, $R_i = 28$ mm, and sandpaper substrate of roughness $\lambda = 540$ μm).

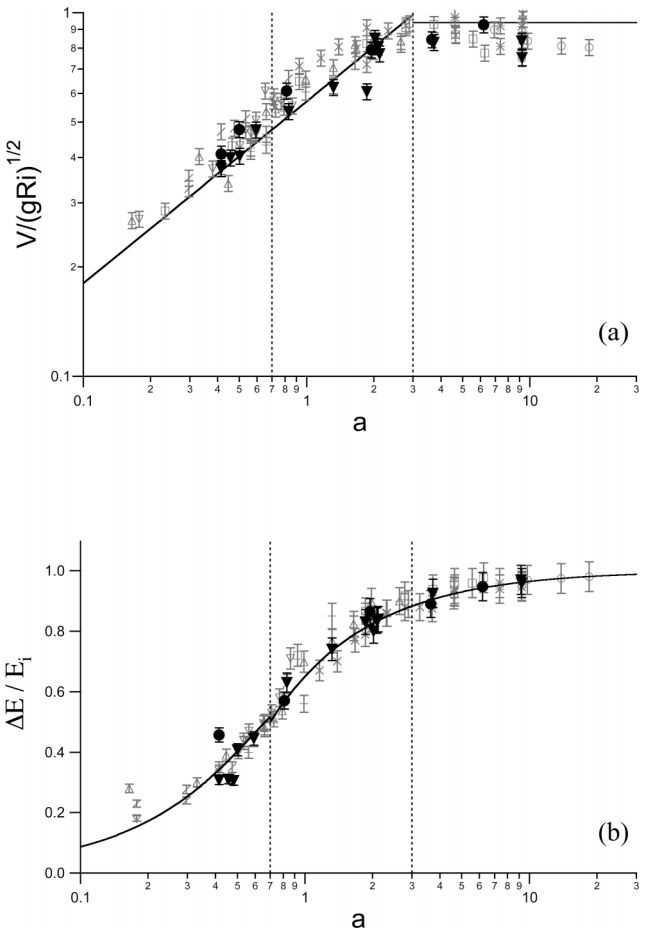

FIG. 9. (a) Rescaled spreading velocity $V/\sqrt{gR_i}$ and (b) proportion of energy dissipated during the flow $\epsilon=\Delta E/E_i$ as a function of a. The different symbols corresponding to the different experimental configurations investigated are detailed in Fig. 6. Data obtained with beads of diameter 350 ± 150 μm spreading on a smooth wooden surface (solid circles) and beads of diameter 1150 ± 150 μm spreading on the rigid sandpaper surface (solid triangles) have been added to (a) and (b). The vertical dotted lines indicate the transitions between the different deposit morphologies. The plain line in (a) corresponds a fit to of the experimental data whereas the plain line in (b) corresponds to the semi-empirical equations (11) and (12).

beads remains blocked in the large holes thus creating an apparent erodible bed of roughness the size of the beads $d=350$ μm. Moreover the spreading of the granular mass essentially involves surface flows so that the properties of the underlying horizontal surface might not significantly affect the spreading velocity.

Fitting the data [plain line in Fig. 9(a)] leads to $V/\sqrt{gR_i}=0.57\sqrt{a}$ as long as $a\lesssim3$ (that is in regime 1). For $a\gtrsim3$ (regime 2), $V/\sqrt{gR_i}$ remains constant on the order of 0.94. In other words, the spreading velocity scales with H_i in the first regime and with R_i in the second regime:

$$a\lesssim3, \quad V=0.57\sqrt{gH_i}, \tag{6}$$

$$a\gtrsim3, \quad V=0.94\sqrt{gR_i}. \tag{7}$$

As H_i remains equal or close to H_f throughout the first regime and since H_f scales with R_i in the second one, Eqs. (6) and (7) essentially suggest that V scales like $\sqrt{gH_f}$ whatever the regime.

Another quantity of interest in order to describe the flow dynamics is the fraction of energy $\epsilon=\Delta E/E_i$ dissipated during the flow, where E_i is the initial gravitational potential energy of the granular column and ΔE is the energy lost during the flow. E_i is simply given by

$$E_i=\frac{MgH_i}{2}=\frac{\pi}{2}\rho_0\phi gR_i^2H_i^2. \tag{8}$$

The granular pile being at rest both at the beginning and at the end of the experiment, the total variation of kinetic energy is 0. The conservation of energy therefore implies $\Delta E=E_i-E_f$, where E_f is the potential energy of the deposit. The latter is easily obtained from the experimentally detected deposit profile $h(r)$ by computing numerically:

$$E_f=2\pi\rho_0\phi g\int_0^{R_f}dr\int_0^{h(r)}dz\,rz. \tag{9}$$

The quantity ϵ was computed for each experimental run. The results are plotted in Fig. 9(b) as a function of a. As with all the other quantities measured up to now, the data collapse on the same curve indicating that ϵ depends neither on the mass released nor on the erodible or rigid nature of the surface but only on a. ϵ increases rapidly with a in the first regime until it saturates at a value close to 1 when entering the second one. In other words, almost all the initial gravitational energy of the granular mass is dissipated by the flow in the second regime.

As already done for R_f, it is possible to estimate the variation of ϵ with a on the basis of geometrical arguments and using Eqs. (1), (2), (4), and (5). For $a<0.74$, the gravitational energy of the deposit is approximately that of a truncated cone of height $H_f=H_i$ and slope θ_r:

$$E_f=\frac{\Pi}{4}H_i^4\left(\frac{1}{\mu_r^2}+\frac{R_f}{H_i}\left(\frac{R_f}{H_i}+\frac{8}{3\mu_r}\right)\right). \tag{10}$$

Using Eq. (4) allows us to eliminate R_f from (10) and leads, after some algebra, to the following expression for ϵ:

$$a<0.74, \quad \epsilon=\frac{a}{6\sqrt{3}\mu_r^2}\sqrt{12\mu_r^2-a^2}. \tag{11}$$

For $a>0.74$, assuming that the deposit has roughly the shape of a cone of height H_f and radius R_f, one gets $E_f=\pi H_f^2R_f^2/12$. Replacing H_f with (2) and R_f with (5) gives the following expression for ϵ:

$$a>0.74, \quad \epsilon=1-\frac{0.74}{2a}. \tag{12}$$

The semi-empirical equations (11) and (12) are plotted in Fig. 9(b) (plain line) and exhibit good agreement with the experimental data.

D. Influence of the roughness of the horizontal surface

Up to now we have been discussing the results of the two first series of experiments involving beads of diameter $d=350\pm50$ μm spreading on rigid or erodible beds of com-

parable roughness. Our main result is that both the flow dynamics and the shape of the deposits depend only on a to leading order. In particular, the flow dynamics and the deposit morphology obtained on an erodible ground are similar to those obtained on a rigid sandpaper surface of roughness $\lambda = 540$ μm. This surprising result might suggest that the underlying ground does not play any role in the spreading of the granular mass. This possibility was briefly investigated through a third series of experiments (series 3) consisting in releasing 350 ± 50 μm glass beads on a wooden board much smoother than the sandpaper substrate. The roughness of the wooden surface is clearly very small compared to the bead size but it was not precisely measured. As a result our analysis of the influence of the ground roughness is essentially qualitative. Keeping this in mind, the wooden substrate will be referred to in the following as the ''smooth ground'' case whereas the sandpaper will sometimes be referred to as the ''rough ground'' case.

Most of the features observed on the sandpaper surface of roughness $\lambda = 540$ μm are recovered on the smooth wooden ground: the same two flow regimes and three deposit morphologies are observed for the same range of a and the shape of the deposit is found not to depend on the released mass M but to vary only with a. Note, however, that the shape of the deposits observed in the smooth ground case differs slightly from that observed in the rough ground case. This is illustrated in Fig. 10 where deposit profiles obtained with $d = 350$ μm beads spreading on the smooth wooden surface (dotted line) are compared to that obtained on the sandpaper substrate (plain line with circles) for each of the three deposit morphologies. At small a, deposit profiles obtained in the rough or in the smooth ground case match relatively well as illustrated by the truncated cone deposit profiles of Fig. 10(a). As a increases, deposits obtained on the smooth ground become progressively different from those obtained on the rough ground [see Figs. 10(b) and 10(c)]. In particular, the deposit height becomes progressively smaller in the smooth ground case. However, and surprisingly, the rescaled radius R_f/R_i of the deposits are identical in the smooth and the rough ground cases, indicating that the radius of the deposit does not depend on the ground roughness. This fact is demonstrated in Fig. 6 where the R_f/R_i data obtained in the smooth ground case (closed circles) are observed to fall on the same curve as data corresponding to the rough ground case. Note that as a result of mass conservation, a shorter final height with a same final radius implies that the flanks of the deposits have to be slightly thicker on the smooth ground than on the rough ground. This feature is easily verified in Figs. 10(b) and 10(c).

Measurements of the spreading velocity $V/\sqrt{gR_i}$ and the fraction of energy dissipated during the flow ϵ in the smooth ground case are found to be in good agreement with the rough ground case, indicating that the flow velocity and the energy dissipated do not depend on the characteristics of the underlying ground. This is illustrated in Figs. 9(a) and 9(b) where the data obtained on the smooth ground (solid circles) have been added to the curve obtained in the rough ground case.

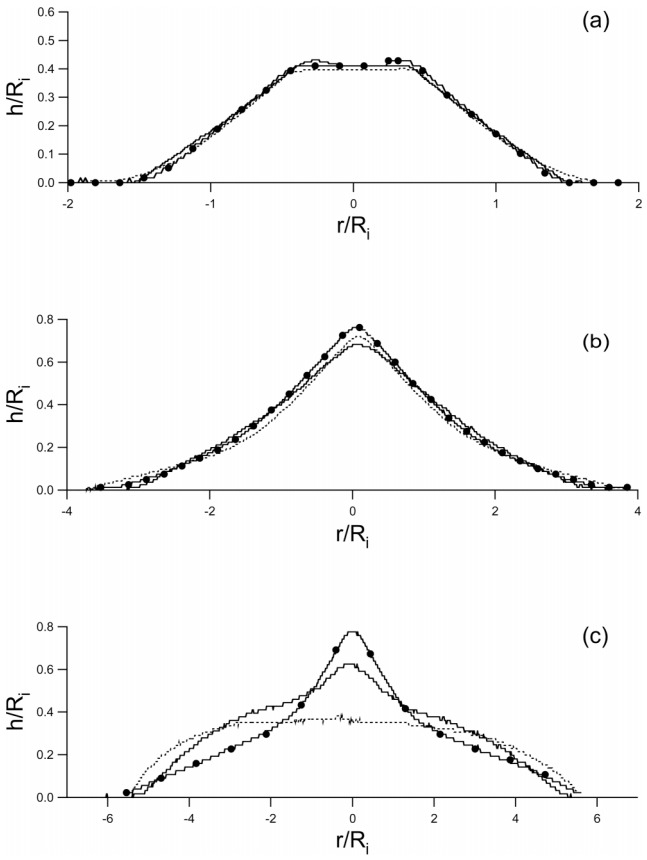

FIG. 10. Deposit profiles normalized to the tube radius. (a) $a = 0.41$. Plain line with circles: $d = 350$ μm, $M = 50$ g, $R_i = 28$ mm, sandpaper substrate of roughness $\lambda = 540$ μm. Dotted line: $d = 350$ μm, $M = 700$ g, $R_i = 70.5$ mm, smooth wooden surface. Plain line: $d = 1150$ μm, $M = 700$ g, $R_i = 70.5$ mm, sandpaper substrate. (b) $a = 1.95$. Plain line with circles: $d = 350$ μm, $M = 600$ g, $R_i = 40$ mm, sandpaper substrate. Dotted line: $d = 350$ μm, $M = 600$ g, $R_i = 40$ mm, smooth wooden surface. Plain line: $d = 1150$ μm, $M = 600$ g, $R_i = 40$ mm, sandpaper substrate. (c) $a = 6.2$. Plain line with circles: $d = 350$ μm, $M = 675$ g, $R_i = 28$ mm, sandpaper substrate. Dotted line: $d = 350$ μm, $M = 675$ g, $R_i = 28$ mm, smooth wooden surface. Plain line: $d = 1150$ μm, $M = 675$ g, $R_i = 28$ mm, sandpaper substrate.

To summarize, the overall shape of the deposit (in particular H_f) appears to depend weakly on the underlying ground roughness in regime 1 where a is small. But this dependency progressively increases with a to become important in the second regime as particularly visible in Fig. 10(c). However the same dynamical regimes and deposit morphologies are recovered for the same range of a values, independent of the substrate roughness. Moreover the rescaled deposit radius R_f/R_i, the rescaled spreading velocity $V/\sqrt{gR_i}$, and the proportion of energy dissipated during the flow, ϵ, are found to be independent of the substrate roughness. These observations are probably a consequence of the fact that the flow essentially develops near the surface of the granular pile so that the flow dynamics are essentially governed by grain/grain interactions and are not affected by the properties of the underlying ground. On a more speculative note we believe that even in the limiting case of a perfectly smooth substrate, the granular mass would not extend indefinitely as dissipation due to grain/grain interactions inside the flowing layer would still suffice to dissipate the flow energy.

In Secs. III B and III C, R_f/R_i and ϵ have been calculated on the basis of semi-empirical arguments such as the knowledge of H_f/R_i. In the present section, we have learned that changing the ground roughness modifies H_f/R_i but does not affect either R_f/R_i or ϵ, in clear contradiction with the discussion leading to Eqs. (4), (5), (11), and (12). Although in good agreement with the experimental data, these equations should therefore not be considered as more than a way to fit the data. Obviously they do not capture the underlying physics of the spreading flow dynamics.

E. Influence of the bead size

The effect of the bead size was investigated by performing a few experiments where glass beads of diameter $d=1150\pm150\,\mu$m were released on the sandpaper substrate of roughness $\lambda\approx540\,\mu$m. The experimental results of this last experimental run are essentially similar to those reported in the previous section. Most of the features observed with beads of diameter $d=350\pm150\,\mu$m are recovered with beads of diameter $d=1150\pm150\,\mu$m: the same flow regimes and deposit morphologies are observed for the same range of a and the shape of the deposit is found not to depend on the released mass M but to vary only with a. The overall shape of the deposits observed with $d=1150\,\mu$m beads slightly differs from that obtained with $d=350\,\mu$m beads as illustrated in Fig. 10: the deposit height is slightly smaller and its flanks are slightly thicker in the $d=1150\,\mu$m beads case. The difference between the two types of deposits increases with a. However, the rescaled deposit radius R_f/R_i, the spreading velocity $V/\sqrt{gR_i}$, and the fraction of energy dissipated during the flow ϵ are found to be identical with $d=350\,\mu$m or $d=1150\,\mu$m. This is demonstrated in Figs. 6(b), 9(a) and 9(b) where the data obtained with $d=1150\,\mu$m beads (solid triangles) are observed to fall on the same curve as the data corresponding to $d=350\,\mu$m. The fact that these quantities do not depend on the bead size is consistent with experimental studies performed in rotating drums which have shown that the material intrinsic properties have little effect on granular surface flow characteristics (especially on the flowing thickness and the shear rate).[15]

IV. CONCLUSION

In this paper, we have been discussing the spreading of a granular mass initially enclosed inside a tube and suddenly released on a horizontal surface. Let us first summarize the experimental observations reported so far.

Two different flow regimes leading to three different deposit morphologies are observed as a function of the initial aspect ratio a, whatever the bead size or the substrate properties (rough or smooth, erodible or rigid). In the first regime, observed for $a\lesssim3$, the granular mass spreads through an avalanche of its flanks dissipating only a fraction of the initial gravitational energy and producing either truncated cone or conical deposits. In the second regime, observed for $a\gtrsim3$, the upper part of the column descends, conserving its shape, while the foot of the pile propagates radially outward. In this second regime, the final deposit looks like a ''Mexican hat;'' almost the totality of the initial gravitational energy is dissipated during the flow and the slope angle at the foot of the deposit is observed to saturate at a value of the order of 5°.

For a given substrate and bead size, the flow dynamics and the shape of the obtained deposits are found to be independent of M but to vary only with the initial aspect ratio a. Systematic measurements of the rescaled deposit height H_f/R_i, the rescaled deposit radius R_f/R_i, the foot and summit angles of the deposit α_f and α_s, the rescaled spreading velocity $V/\sqrt{gR_i}$, and the rate of energy dissipated during the flow $\Delta E/E_i$ reveal that these quantities do not depend on M but vary only with a. We provide experimental scaling laws for these data but accounting theoretically for these laws is beyond the scope of the present paper. However, the experimental data suggest that upon removal of the tube the granular cylinder pile undergoes an active Coulomb-yielding process and yields to the stress modification by failing along a surface of angle $\theta_y=\tan^{-1}(0.74)\approx36.5°$ and developing a surface flow.

Further investigation indicates that the overall shape of the deposit (in particular H_f, α_f and α_s) depends only slightly on the substrate properties (smooth or rough, rigid or erodible) and on the bead size in regime 1 where a is small. But this dependency progressively increases with a to become eventually important in the second regime. However the same dynamical regimes and deposit morphologies are recovered for the same range of a, independent of the substrate properties or the bead size. Moreover the rescaled deposit radius R_f/R_i, the rescaled spreading velocity $V/\sqrt{gR_i}$, and the fraction of energy dissipated during the flow, ϵ, do not depend on the substrate properties, the bead size, and the released mass M, but vary only with a. This constitutes the most striking result of this paper. We believe that the independance of these quantities with respect to the substrate properties is due to the fact that the flow develops near the free surface of the granular pile. As a result, the flow dynamics is essentially controlled by grain/grain interactions independent of the underlying substrate properties. Moreover, experimental studies performed in rotating drums have shown that the material intrinsic properties have little effect on granular surface flow characteristics (especially on the flowing thickness and the shear rate),[15] a fact that might explain why our results are independent of the bead size. The absence of dependence of the flow properties and the deposit morphologies with the released mass M remains a puzzling result.

At the time we were finishing this paper, we became aware of some similar experiments presented in a talk given by H. Huppert at the Granular and Particle-laden Flows Workshop that was held at the Isaac Newton Institute in November 2003.[16] The authors studied experimentally the collapse of an initial cylinder of granular matter onto a horizontal base. The observations they reported seem to confirm our own results with one exception: contrary to these authors, we do observe an influence of both the underlying ground properties and the bead size on the morphology of the deposit, particularly when a becomes large enough. A possible explanation of this apparent contradiction between our two experimental studies might be that the roughness of the different

substrates used in the experiments of Huppert *et al.* always remained very small compared to the typical grain size and was never large enough to affect the experimental results.

Returning to the context of geophysical granular flows, large rock avalanches are commonly described by their relative runout length defined as the ratio of the runout distance to the fall height. This relative runout length show a tendency to increase with volume from a value of about 2 at volumes smaller than $10^5\,m^3$ to values larger than 10 for volume in excess of 1 km^3. However this trend exhibits a large scatter, the origin of which remains controversial.[1,17] Our experimental results suggest the possibility that the initial aspect ratio of the granular mass (before collapsing) might affect the runout length, at least in the case where this mass flows along a small slope, and therefore contributes to the scatter observed in the field measurements.

ACKNOWLEDGMENTS

We thank G. Bienfait, Y. Gamblin, K. Mahiouz, and A. Viera for their invaluable technical assistance in designing and realizing the experimental setup. We are indebted to R. Guise for his contribution to the experimental work. We also thank O. Dauchot, S. Douady, P. Gondret, F. Metivier, O. Pouliquen, and all the members of the GDR Midi for many fruitful discussions. This is IPGP contribution No. 1974.

[1] R. Iverson, ''The physics of debris flows,'' Rev. Geophys. **35**, 245 (1997).
[2] R. Iverson and J. Vallance, ''New views on granular mass flows,'' Geology **29**, 115 (2001).
[3] K. Hutter, T. Koch, C. Pluss, and S. Savage, ''The dynamic of avalanches of granular materials from initiation to runout. II. Experiments,'' Acta Mech. **109**, 127 (1995).
[4] O. Pouliquen, ''Scaling laws in granular flows down rough inclined planes,'' Phys. Fluids **11**, 542 (1999).
[5] O. Pouliquen and Y. Forterre, ''Friction law for dense granular flows: Application to the motion of a mass down a rough inclined plane,'' J. Fluid Mech. **453**, 131 (2002).
[6] S. B. Savage and K. Hutter, ''The motion of a finite mass of granular material down a rough incline,'' J. Fluid Mech. **199**, 177 (1989).
[7] A. Mangeney-Castelnau, J. Vilotte, M. Bristeau, B. Perthame, F. Bouchut, C. Simeoni, and S. Yerneni, ''Numerical modeling of avalanches based on Saint-Venant equations using a kinetic scheme,'' J. Geophys. Res. (in press).
[8] M. Naaim, S. Vial, and R. Couture, *St Venant Approach for Rock Avalanches Modelling in Multiple Scale Analyses and Coupled Physical Systems*, Volume St-Venant Symposium (Presse de l'Ecole Nationale des Ponts et Chausses, 1997).
[9] A. Mangeney, P. Heinrich, R. Roche, G. Boudon, and J. L. Chemine, ''Modeling of debris avalanche and generated water waves: Application to real and potential events in Montserrat,'' Phys. Chem. Earth **25**, 741 (2000).
[10] E. Pitman, C. Nichita, A. Patra, A. Bauer, M. Sheridan, and M. Bursik, ''Computing granular avalanches and landslides,'' Phys. Fluids **15**, 3638 (2003).
[11] T. Boutreux and P. de Gennes, ''Evolution of a step in a granular material: The Sinai problem,'' C. R. Acad. Sci., Ser. IIb: Mec., Phys., Chim., Astron. **325**, 85 (1997).
[12] J. Bouchaud, M. Cates, J. Prakash, and S. Edward, ''A model for the dynamics of sandpile surfaces,'' J. Phys. I **4**, 1383 (1994).
[13] A. Daerr and S. Douady, ''Sensitivity of granular surface flows to preparation,'' Europhys. Lett. **47**, 324 (1999).
[14] A. Mangeney, P. Heinrich, and R. Roche, ''Analytical solution for testing debris avalanche numerical models,'' Pure Appl. Geophys. **157**, 1081 (2000).
[15] G. D. R. Midi, ''On dense granular flows,'' Eur. Phys. J. E. (in press).
[16] H. Huppert, G. Lube, S. Sparks, and M. Hallworth, ''Axisymmetric granular collapse,'' Granular and Particle-laden Flows Workshop, Isaac Newton Institute for Mathematical Sciences, Cambridge, UK, 2003.
[17] F. Legros, ''The mobility of long-runout landslides,'' Eng. Geol. (Amsterdam) **63**, 301 (2002).